Human Molecular Genetics, 2011, Vol. 20, No. 8 **1467–1477**
doi:10.1093/hmg/ddr025
Advance Access published on January 21, 2011

The N-terminal region of centrosomal protein 290 (CEP290) restores vision in a zebrafish model of human blindness

Lisa M. Baye[1], Xiaobai Patrinostro[1], Svetha Swaminathan[1], John S. Beck[2,4], Yan Zhang[2,4], Edwin M. Stone[3,4], Val C. Sheffield[2,4] and Diane C. Slusarski[1,*]

[1]Department of Biology, [2]Department of Pediatrics and [3]Department of Ophthalmology and Visual Sciences, University of Iowa, Iowa City, IA, USA and [4]Howard Hughes Medical Institute, Chevy-Chase, MD, USA

Received December 14, 2010; Revised and Accepted January 18, 2011

The gene coding for centrosomal protein 290 (CEP290), a large multidomain protein, is the most frequently mutated gene underlying the non-syndromic blinding disorder Leber's congenital amaurosis (LCA). *CEP290* has also been implicated in several cilia-related syndromic disorders including Meckel–Gruber syndrome, Joubert syndrome, Senor–Loken syndrome and Bardet–Biedl syndrome (BBS). In this study, we characterize the developmental and functional roles of *cep290* in zebrafish. An antisense oligonucleotide [Morpholino (MO)], designed to generate an altered *cep290* splice product that models the most common LCA mutation, was used for gene knockdown. We show that *cep290* MO-injected embryos have reduced Kupffer's vesicle size and delays in melanosome transport, two phenotypes that are observed upon knockdown of *bbs* genes in zebrafish. Consistent with a role in cilia function, the *cep290* MO-injected embryos exhibited a curved body axis. Patients with LCA caused by mutations in *CEP290* have reduced visual perception, although they present with a fully laminated retina. Similarly, the histological examination of retinas from *cep290* MO-injected zebrafish revealed no gross lamination defects, yet the embryos had a statistically significant reduction in visual function. Finally, we demonstrate that the vision impairment caused by the disruption of *cep290* can be rescued by expressing only the N-terminal region of the human CEP290 protein. These data reveal that a specific region of the CEP290 protein is sufficient to restore visual function and this region may be a viable gene therapy target for LCA patients with mutations in *CEP290*.

INTRODUCTION

Mutations in *centrosomal protein 290* (*CEP290*) cause the non-syndromic blinding disorder Leber's congenital amaurosis (LCA10, OMIM 611755) as well as several cilia-based syndromic disorders including Meckel–Gruber syndrome (MKS4, OMIM 611134), Joubert syndrome (JSTS5, OMIM 610188), Senor–Loken syndrome (SLSN6, OMIM 610189) and Bardet–Biedl syndrome (BBS14, OMIM 209900). The CEP290 protein is encoded by 54 exons, is 2479 amino acids in length and has 25 predicted protein domains, motifs and localization signals (1). Disease-causing mutations including missense, nonsense, splicing and frame shifting changes occur throughout the length of the protein (2,3). To date, no clear correlations between phenotype and the corresponding genotype have been identified between *CEP290* mutations and observed diseases (2); therefore, it has been difficult to understand the precise role and the functional domains of this large protein. Moreover, although these diseases have some overlapping phenotypes, there is variability in the severity of disease states and organ involvement, which is consistent with the idea that the protein has tissue-specific roles that manifest differently based on the genotype.

*To whom correspondence should be addressed at: Department of Biology, University of Iowa, 246 Biology Building, Iowa City, IA 52242, USA. Tel: +1 3193353229; Fax: +1 3193351069; Email: diane-slusarski@uiowa.edu

The CEP290 protein has been shown to play a role in microtubule-associated protein transport and localizes to centrioles as well as to the connecting cilium of the photoreceptor cell (1,4). The photoreceptor is a highly polarized, light-sensing cell of the retina. The cell body, where protein synthesis occurs, is found in the outer nuclear layer and is connected to the outer segment, where phototransduction occurs, via a modified cilium called the connecting cilium. The connecting cilium transports proteins critical for development, maintenance and function of the photoreceptor from the cell body to the outer segment through the process of intraflagellar transport (5–10). Changes or disruptions in proper protein trafficking have been shown to result in photoreceptor degeneration and ultimately blindness (9,11,12). LCA is an early-onset blinding disorder in which most patients present in infancy with a lack of visual response but relatively normal retina (13–15). Mutations in *CEP290* account for up to 30% of all LCA cases, and the most common *CEP290* mutation accounts for ~43% of the disease-causing variations in this gene (13,15,16). This common *CEP290* allele is an intronic mutation that disrupts normal splicing of the transcript resulting in a premature stop codon; however, this particular mutation is considered hypomorphic as some wild-type transcript is still present in the homozygous affected individuals (17).

Two genetic animal models are currently being used to study the role of CEP290 in vision, the *rd16* mouse and the rdAc cat. The *rd16* mouse possesses an in-frame deletion of amino acids 1599–1897 and presents with a severe, early-onset retinal degeneration that exhibits decreased rod and cone function by post-natal day 18 (4). The rdAc cat harbors an intronic mutation that causes an aberrant splicing of the transcript in intron 50 resulting in a truncated protein that is missing the last 159 amino acids (18). rdAc cats exhibit late-onset retinal degeneration (18). The variation in the phenotypes observed between these animal models of LCA with unique genotypes led us to examine the developmental role of *cep290* relative to vision in the zebrafish system by specifically targeting a region of the *cep290* gene that would model the most common human *CEP290* mutation causing LCA in patients, c.2991 + 1655A > G (17). We then performed structural/functional analysis of CEP290 by testing the sufficiency of specific regions of the human CEP290 protein to suppress gene knockdown defects. Finally, we tested the ability of these regions to bind nephronophthisis-2 (NPHP2), a known member of complexes in the retina proposed to affect retinal degeneration (19).

cep290 knockdown in zebrafish has been previously shown to result in several phenotypes including convergence extension defects, hydrocephalus, small eyes, kidney cysts and body curvature (1,20–22). In our targeted knockdown of *cep290* in zebrafish, we observed curvature of the body axis indicative of cilia dysfunction. Mutation of *CEP290* has been reported in a single individual with phenotypic features overlapping BBS (resulting in the alternative gene name *BBS14*). We evaluated our *cep290* knockdown embryos and found that they exhibited two phenotypes shared when all *bbs* genes are knocked down to date (*bbs1–13*) in zebrafish, reduced Kupffer's vesicle (KV) size and delayed retrograde melanosome transport (23–26) (Lisa M. Baye and John S. Beck, unpublished data). Histological examination of the developing retina in *cep290* knockdown embryos revealed no gross lamination defects; however, functional analysis of vision revealed a reduction in visual behavior. Importantly, we were able to restore visual responsiveness by expressing only the N-terminal region of the human CEP290 protein in the knockdown embryos. This observation indicates that the N-terminal region of the *CEP290* gene is sufficient to suppress the visual impairment and may be a viable treatment option for LCA patients.

RESULTS

cep290 is expressed throughout development in several tissues including the KV and eye

To understand the functional role of *cep290* in the zebrafish, we first examined the spatial–temporal expression pattern of the gene throughout development and in adult tissues. Reverse transcriptase–polymerase chain reaction (RT–PCR) analysis revealed that the *cep290* transcript is inherited maternally and is present throughout all stages of development (Fig. 1A). *cep290* is also expressed in the adult zebrafish eye and, specifically, in the retina (Fig. 1A) as well as in all other tissues examined (data not shown). Whole-mount *in situ* hybridization at the 8-somite stage shows that the gene is ubiquitously expressed early in development (Fig. 1B and C). Of note, *cep290* is present around the KV (Fig. 1D), which is a ciliated structure found transiently in the posterior tailbud and contributes to left–right patterning of the embryo (27). In 5-day post-fertilization (dpf) embryos, *cep290* is found in several tissues including the brain, eye, ear, notochord and the gut region when compared with the control embryo with no antisense probe added (Fig. 1E and F). Sectioning of the 5 dpf retina revealed *cep290* expression in the ganglion cell layer (GCL), portions of the inner nuclear layer (INL) as well as the photoreceptor cell layer (PR) (Fig. 1G and H).

cep290 gene targeting and gross morphology of knockdown embryos

The most common human *CEP290* mutation underlying LCA is an intronic mutation, c.2991 + 1655A > G, which alters gene splicing and results in a stop at amino acid C998X (Fig. 2A) (17). We mimicked this LCA mutation in zebrafish by using an antisense Morpholino (MO) that disrupts the splicing of the zebrafish *cep290* transcript at the corresponding exon 25 leading to intron inclusion (Fig. 2A, hashed bar).

cep290 MO-injected embryos (morphants) exhibit body curvature defects in a MO dose-dependent manner ranging from straight to a severe C-shaped (curly) axis at 5 dpf (Fig. 2B). The curly body shape is similar to that observed in the cilia mutant *seahorse*, as well as in previously published *cep290* exon 42-targeted knockdown zebrafish embryos (21,28). This body morphology defect is consistent with our observation that the *cep290* transcript is expressed in the developing notochord (Fig. 1F). Embryos injected with the highest dose of MO (10 ng) had the greatest percentage of curly embryos (80%), whereas only 34% of embryos injected with

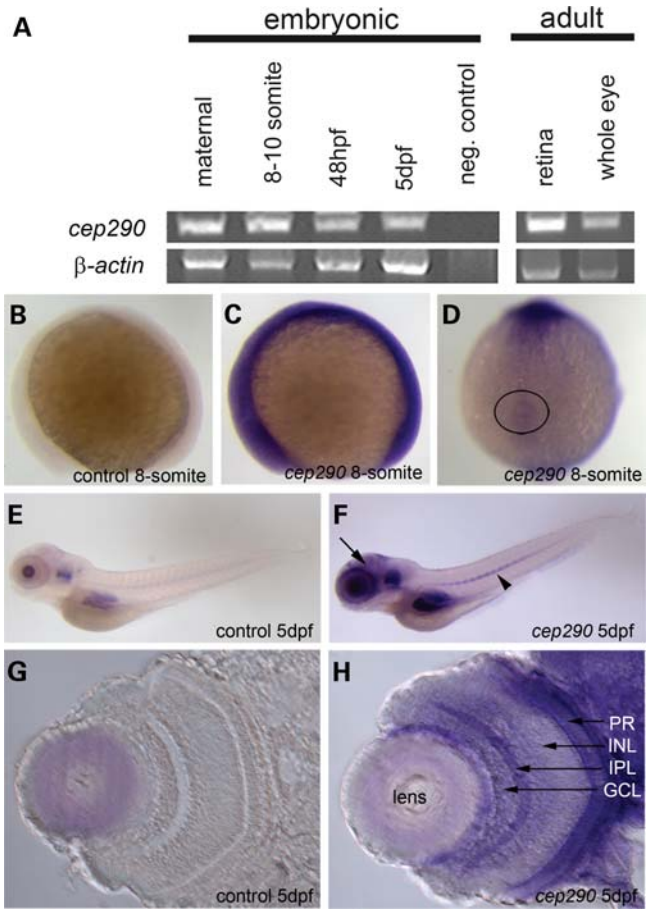

Figure 1. *cep290* transcript expression throughout development and in adult tissues. (**A**) RT–PCR of the *cep290* transcript in wild-type embryos showing expression at all the stages and tissues examined: maternal, 8–10 somites, 48 hpf, 5 dpf, adult retina and adult whole eye. *β-actin* expression served as a loading control. (**B**–**H**) Whole-mount *in situ* hybridization using an antisense probe corresponding to a portion of the *cep290* gene (see Materials and methods). Control embryos had no *cep290* antisense probe added to the reaction. (B and C) Side view of a control and *cep290* hybridized embryos at 8-somites. The *cep290* transcript is present ubiquitously. (D) Dorsal view of the 8-somite embryo revealing that *cep290* is expressed around the KV (circle). (E and F) Side view of a control and *cep290* hybridized embryos at 5 dpf. The *cep290* transcript is present in several tissues including the brain (arrow) and notochord (arrowhead). (G and H) Transverse sections of the eye at 5 dpf. The *cep290* transcript is present in the GCL, portions of the INL and the PR cells. GCL, ganglion cell layer; IPL, inner plexiform layer; INL, inner nuclear layer; PR, photoreceptors.

low-dose (5 ng) MO presented with the curly body axis (Table 1).

To verify disrupted splicing in the straight body morphant embryos, primers were designed to flank intron 25 (Fig. 2A). MO-injected embryos (8 ng dose) with a straight body axis were pooled for RNA isolation and RT–PCR was performed. Uninjected embryo cDNA amplified the expected wild-type transcript (Fig. 2C). *cep290* MO-injected embryos presented a larger transcript consistent with intron inclusion (Fig. 2C). Indeed, sequence analysis of the product revealed inclusion of intron 25 which generates a frame shift that introduces a stop six amino acids past the coding amino acid 1018 in the zebrafish transcript (Fig. 2A). This aberrant transcript is present from the 8–10-somite stage through 5 dpf (Fig. 2C). Additionally, some wild-type transcript is present in the morphant embryos, and we posit that having some wild-type transcript indeed makes this model more similar to LCA patients with the hypomorphic c.2991 + 1655A > G mutation.

cep290 morphants have the cardinal zebrafish BBS phenotypes

We have previously described cilia- and transport-related defects observed with the knockdown of *bbs* genes in zebrafish (23–26). All *bbs* genes tested resulted in abnormal KV size and delayed retrograde melanosome transport in the skin pigment; therefore, we examined these cardinal features in *cep290* morphant embryos (23–26).

The KV is a ciliated organ found transiently in the posterior tailbud of developing embryos from 6–15 somites (Fig. 3A). The size of the KV is assessed at the 8–12-somite stage by comparing the vesicle width to the width of the developing notochord. Embryos with a KV larger than the width of the notochord are considered normal (Fig. 3B), whereas a KV that is the same size or smaller than the width of the notochord is considered abnormal (Fig. 3C). We determined that the knockdown of *cep290* results in a statistically significant percentage of embryos with abnormally sized KVs, 20.8% at the 10 ng dose, compared with 5.6% of wild-type (Fisher's exact test, $^{**}P < 0.01$; Fig. 3D). The percentage of embryos with abnormal KVs increased in a MO dose-dependent manner.

The second cardinal feature of BBS assessed in zebrafish was the rate of melanosome movement, which is a method to examine intracellular transport. Under standard conditions, zebrafish embryos adapt to their environment by trafficking their melanosomes (pigment) within the melanophores in response to light and/or hormonal stimuli (29–31). The average time of melanosome transport is assessed by treating 5 dpf dark-adapted embryos with epinephrine to chemically stimulate movement. Dark adaptation maximally disperses the melanosomes throughout the melanophore (Fig. 3E and F), whereas epinephrine treatment results in rapid retrograde movement of melanosomes to the perinuclear region (Fig. 3G) (23–26,32). Completion of melanosome transport in wild-type embryos averages 1.58 min, whereas *cep290* morphant embryos at all doses showed a statistically significant delay with the 10 ng dose averaging 2.50 min (Fig. 3H, ANOVA with Tukey, $^{*}P < 0.05$, $^{**}P < 0.01$). Together, these data indicate that the knockdown of the *cep290* transcript results in the cardinal BBS phenotypes in the zebrafish supporting a role for CEP290 in some patients with BBS.

cep290 morphants exhibit a vision defect with normal retinal lamination

To assess the role of *cep290* in the developing retina, we performed histological analysis by hematoxylin and eosin (H&E) staining of morphant embryos at 3 and 5 dpf. For these analyses, we selected the moderate MO dose (8 ng) because it led to intron inclusion through 5 dpf (Fig. 2C) and displayed both the straight and the curved body axis phenotypes (Fig. 2B). We determined that regardless of body curvature, morphant embryos had a fully laminated retina at 3 dpf (Fig. 4C and D). Additionally, the photoreceptor outer

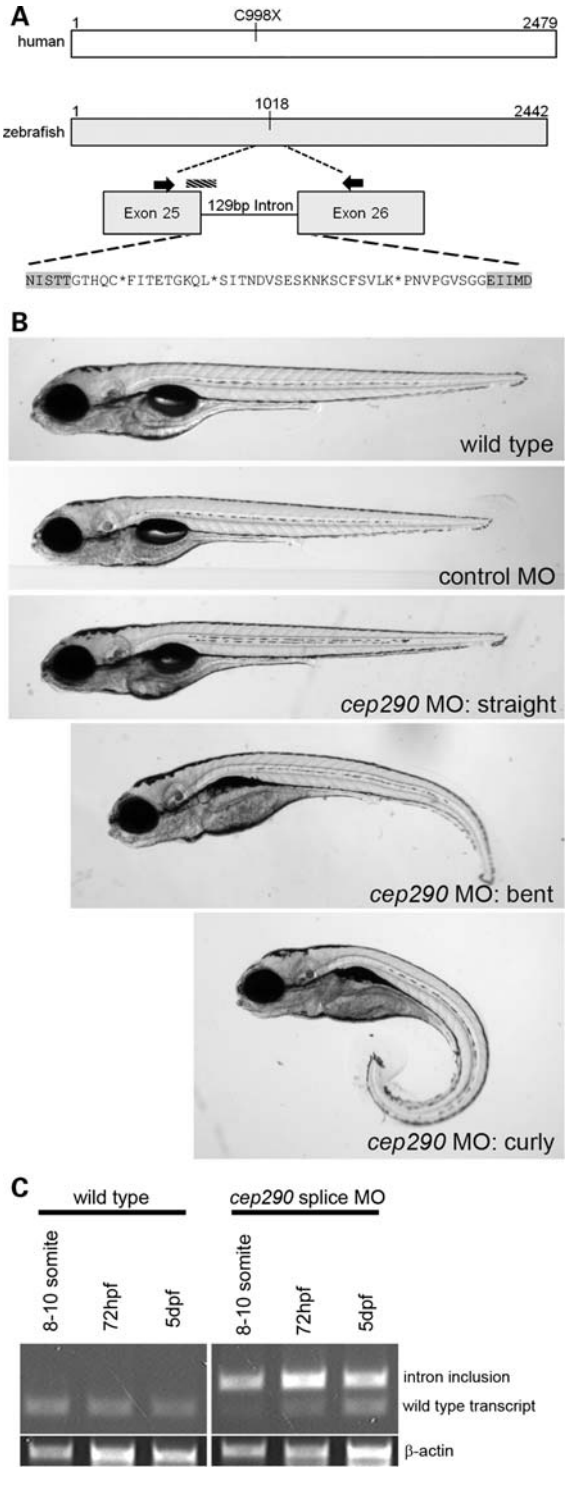

Figure 2. *cep290* gene targeting and gross morphant phenotypes. (**A**) Schematic of full-length human (white) and zebrafish (gray) CEP290 proteins. The most common CEP290 mutation in LCA patients (C998X) is noted. The location of the splice-blocking MO is depicted by the hashed bar and the flanking primers used for RT–PCR are shown with black arrows. The open reading frame for the region of interest is depicted with amino acids highlighted in gray representing the sequence from exons 25 and 26 flanking the included intron sequence that begins at amino acid 1018. Asterisks represent the stop codons. (**B**) Live images of 5 dpf wild-type, control-injected and *cep290* morphant embryos representing the range of gross morphology observed. MO-injected embryos presented with body plans that were straight, bent or curly in a MO dose-dependent manner (Table 1). (**C**) RT–PCR from wild-type and *cep290* morphant embryos injected with 8 ng of MO at the following stages: 8–10 somites, 72 hpf and 5 dpf. Only morphants with a straight body axis at 72 hpf and 5 dpf were used to assess the gene knockdown. The aberrantly spliced *cep290* transcript in morphant embryos (intron inclusion) is present through 5 dpf. *β-actin* expression served as a loading control.

Table 1. Percentages of embryos with body curvature defects based on MO dose

Experimental group	Phenotype (percentage)			*n*
	Straight	Bent	Curly	
Wild-type	100	0	0	129
cep290 MO (5 ng)	60	6	34	205
cep290 MO (8 ng)	40	5	55	282
cep290 MO (10 ng)	13	7	80	208

segments in the central retina revealed no overt differences compared with wild-type and control-injected embryos (Fig. 4G and H). In contrast to the parallel organization of the extending outer segments in wild-type and control-injected embryos, the extending outer segments of *cep290* morphants appeared more wavy, suggesting modest disorganization at 5 dpf (Fig. 4K and L).

Since patients with LCA caused by mutations in *CEP290* have been shown to present with and maintain a fully laminated retina and sparing of some photoreceptor cells yet has reduced visual perception, we sought to functionally assess vision in the *cep290* morphants (14,33). To evaluate visual function in zebrafish, we utilized a natural escape response that is elicited when embryos are exposed to rapid changes in light intensity (26,34,35). In the vision assay, visually responsive 5 dpf embryos change their swimming behavior when there is a short block in a bright light source (Fig. 4M–O, Supplementary Material, Movies S1 and S2). The assay is repeated five times spaced 30 s apart, and the average number of responses is reported. Wild-type embryos respond an average of 3.53 times (Fig. 6). As a control for the assay, the visually impaired *cone-rod homeobox* (*crx*) morphant embryos were utilized and responded only 2.00 times (Fig. 6) (26,35). Only *cep290* morphant embryos that possessed a straight body axis were used for this behavioral assay to ensure uncompromised locomotor activity (Supplementary Material, Fig. S1). In contrast to wild-type and control MO-injected embryos, *cep290* morphants responded only 2.46 times during the five trials (ANOVA with Tukey, $P < 0.01$). The range of responses for each experimental set of embryos is depicted in Supplementary Material, Figure S2. The majority of wild-type and control MO-injected embryos, 67 and 54%, respectively, responded 4–5 times in the assay of five trials, whereas only 19% of the *cep290* morphants and 16% of the *crx* morphants responded as many times. These observations indicate that the *cep290* morphant embryos have reduced visual activity.

N- and C-terminal truncation constructs of CEP290 localize to centrioles

Having shown that *cep290* morphant embryos have overall normal retina histology but still present with a vision defect,

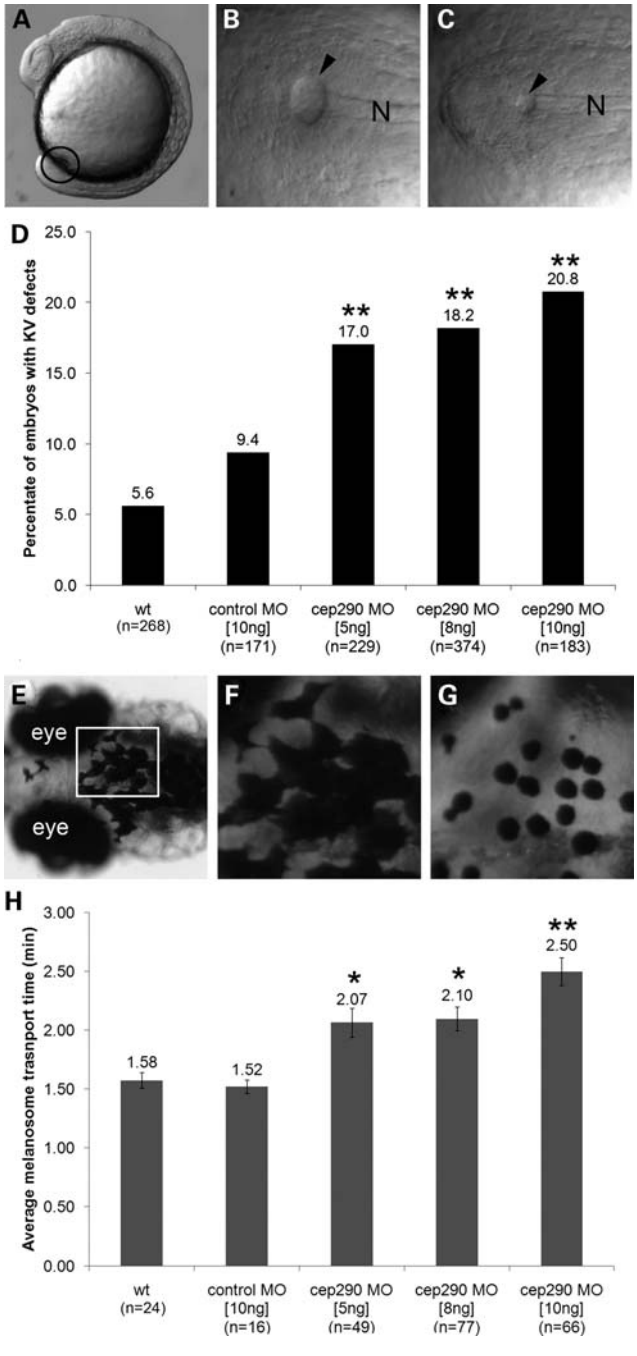

Figure 3. *cep290* gene knockdown results in zebrafish BBS cardinal features. (**A**) Side view of a 10-somite embryo highlighting the location of the ciliated KV (circle) in the tailbud. (**B** and **C**) Dorsal views of an average-sized KV and an abnormally reduced in KV size, respectively, (arrow heads) at the 10-somite stage. The notochord is marked with an 'N'. Embryos were scored has having an abnormal KV if the vesicle was less than the width of the notochord. (**D**) The percentage of wild-type, control-injected and *cep290* morphant embryos with abnormal KVs. MO concentration and the number of embryos (*n*) are noted on the *x*-axis. $^{**}P < 0.01$, Fisher's exact test when compared with wild-type. (**E**) Dorsal view of the head melanocytes of a 5 dpf dark-adapted wild-type embryo. The boxed region represents the zoomed region for **F** and **G**. (F) Dark-adapted melanocytes prior to epinephrine treatment note the dispersed melanosomes. (G) The end point, perinuclear localization of melanosomes, after epinephrine treatment. (**H**) Epinephrine-induced retrograde transport times for wild-type, control-injected and *cep290* morphants. MO concentration and the number of embryos (*n*) are noted on the *x*-axis. $^{*}P < 0.05$, $^{**}P < 0.01$, ANOVA with Tukey when compared with wild-type.

we next used this vision assay to functionally identify regions of the CEP290 protein that are sufficient to suppress the vision defect. Indeed, if a smaller portion of this protein is sufficient to restore vision, then it alone could be used for gene therapy in patients using the standard retroviral techniques that are currently available. We, therefore, divided the human *CEP290* gene into an N-terminal fragment that represents the first 1059 amino acids of the protein (Fig. 5A, blue) and a C-terminal fragment, amino acids 1765–2479 (Fig. 5A, green). Both of these constructs contain regions that have previously been shown to form multimers by homodimerization (21). The N-terminal construct extends over the region where the most common LCA mutation is found (noted in Fig. 5A). The C-terminal construct contains a large portion of the predicted myosin-tail domain of CEP290 that has been hypothesized to play a vision-specific role as this region is partially deleted in the *rd16* mouse model of retinal degeneration (deletion of amino acids 1599–1897) (4). Additionally, this construct covers the entire region that is truncated in the rdAc cat model of late-onset retinal degeneration (18).

We first evaluated expression and localization of the human CEP290 N- and C-terminal constructs in zebrafish. mRNA encoding myc-tagged fusion constructs were injected into zebrafish embryos and immunohistochemistry was performed. Immunostaining using anti-myc antibody revealed the expression of the constructs at 50% epiboly [~6 hpf (hours post-fertilization); Fig. 5B and E]. Since full-length CEP290 localizes closely with the centrioles in tissues and cell lines (1,4), zebrafish centrin fused to green fluorescent protein (eGFP) was co-injected as a marker for the centriole (Fig. 5C, F and I). With both the N-terminal and the C-terminal constructs, we observed some paracentriolar as well as cytoplasmic localization (Fig. 5D and G). To verify the localization of the proteins in ciliated cells, we expressed the N-terminal and the C-terminal constructs in undifferentiated and ciliated ARPE-19 cells and found both constructs to be paracentriolar (Supplementary Material, Figs S3 and S4).

N-terminal region sufficient to rescue the vision defect

We next assessed if the human constructs can function in zebrafish to rescue the MO-induced vision defect. Embryos co-injected with *cep290* MO and the mRNA encoding myc-tagged N- and C-terminal constructs were grown to 5 dpf. Again, only morphant embryos with a straight body axis were used in the vision assay to ensure proper embryo motility (Supplementary Material, Fig. S1). In the vision assay, *cep290* morphant embryos responded on average 2.46 times, whereas morphant embryos injected with the N-terminal CEP290 construct responded 3.48 times (Fig. 6). This response was statistically the same as the wild-type response of 3.53, indicating the rescue of the MO-induced vision defect. The number of *cep290* morphant embryos injected with the N-terminal construct that now responded 4–5 times in the assay rose to 53% from 19% in the MO alone (Supplementary Material, Fig. S2). Conversely, injection of the C-terminal construct was unable to rescue the vision defect (Fig. 6; ANOVA with Tukey, $^{**}P < 0.01$). Neither the N-terminal nor the C-terminal construct was sufficient to rescue the KV size defect and only

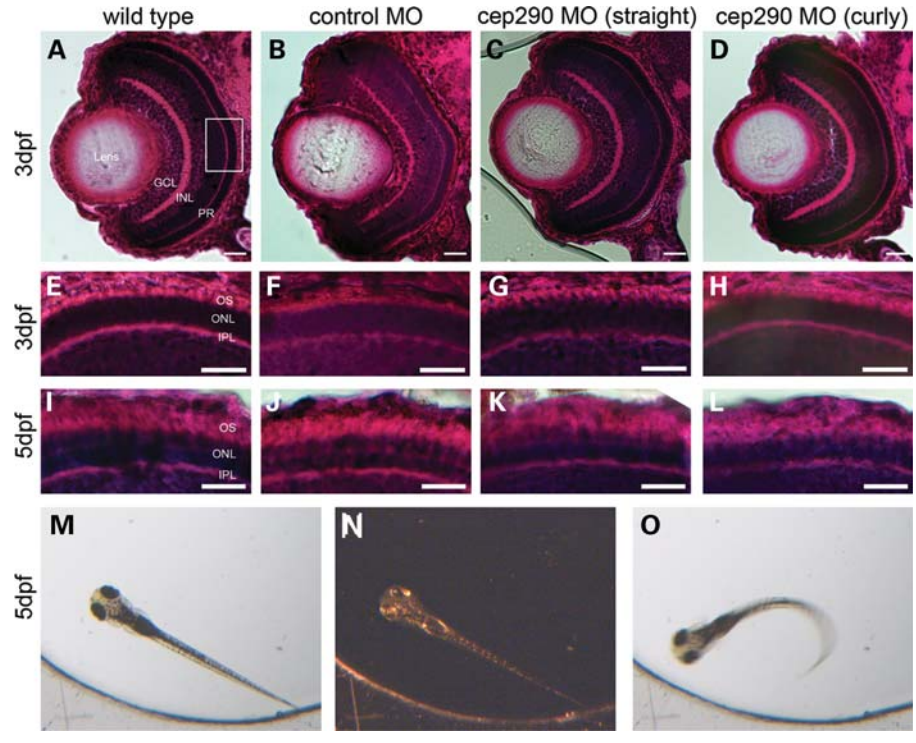

Figure 4. Retinal histology and functional analysis of vision in *cep290* morphants. (**A**–**L**) H&E staining of transverse retinal cryosections of wild-type, control-injected and *cep290* morphants with a straight or curly body axis. Scale bars = 10 μm. (A–D) Whole eye images of 3 dpf wild-type, control-injected and *cep290* MO-injected embryos. The lens, GCL, INL and PR are labeled in (A). The white box represents the central region of the retina that was examined at higher magnification in (E)–(L). (E–H) Zoom of PR cell layer in the central retina at 3 dpf. (I–L) Zoom of PR cell layer in the central retina at 5 dpf. ONL, outer nuclear layer; IPL, inner plexiform layer; OS, outer segments of the photoreceptor cells. (**M**–**O**) Selected image from a time-lapse movie generated while performing the vision startle response assay to test the visual function of 5 dpf embryos. (M) Embryo in bright light illumination. (N) A 1 s block in light. Image has been contrast manipulated in Adobe Photoshop to visualize embryo. (O) Characteristic C-bend swimming behavioral response observed when the bright light illumination is turned back on.

the C-terminal construct showed a suppression of the melanosome transport delay (Table 2). Taken together, these data indicate that the N-terminal region of the human *CEP290* gene is sufficient to rescue the *cep290* MO-induced vision defect. Additionally, because the N-terminal region cannot rescue KV and melanosome transport defects, this indicates that other regions of the protein are needed for these cellular functions.

The N-terminal region of CEP290 binds NPHP2

It has been shown in the retina that several NPHP proteins, including CEP290 (also known as NPHP6), form protein complexes that interact with retinitis pigmentosa GTPase regulator (RPGR), a protein known to affect retinal function (19). Additionally, NPHP5 has been shown to directly bind a region found within our N-terminal fragment of CEP290, and mutations in NPHP5 cause some cases of the syndromic blinding disorder renal–retinal SLSN (21,36). To explore a mechanism by which the N-terminal region of CEP290 may function in vision, we examined whether another NPHP complex component in the retina, NPHP2, binds to either the N-terminal or the C-terminal regions of CEP290 (19). Like NPHP5, a mutation in NPHP2 has also been associated with vision impairment (37). By transient transfection and co-immunoprecipitation (IP) assays, we find that the N-terminal, but not the C-terminal, region of CEP290 physically interacts with NPHP2 (Fig. 7). These results provide further evidence that the N terminus of CEP290 interacts with a known protein complex necessary for vision.

DISCUSSION

CEP290 has been associated with several cilia-related diseases, but the precise functional domains of the protein and their role in normal development need to be determined. We observed that the *cep290* transcript is present throughout all stages of zebrafish embryo development and is enriched in the KV region as well as in ganglion cells, the INL and photoreceptor cells of the retina. Using a targeted knockdown strategy to model the most common *CEP290* mutation in LCA patients, we found body curvature defects, KV size reduction, delayed retrograde melanosome transport and vision impairment. We determined by using truncated CEP290 constructs that the N-terminal region of the CEP290 protein is sufficient to rescue the vision defect observed in *cep290* knockdown embryos. Finally, we determined that this N-terminal region of the protein, but not the C-terminal region, can bind NPHP2.

LCA patients with the c.2991 + 1655A > G mutation are hypomorphic in that some wild-type transcript is present in

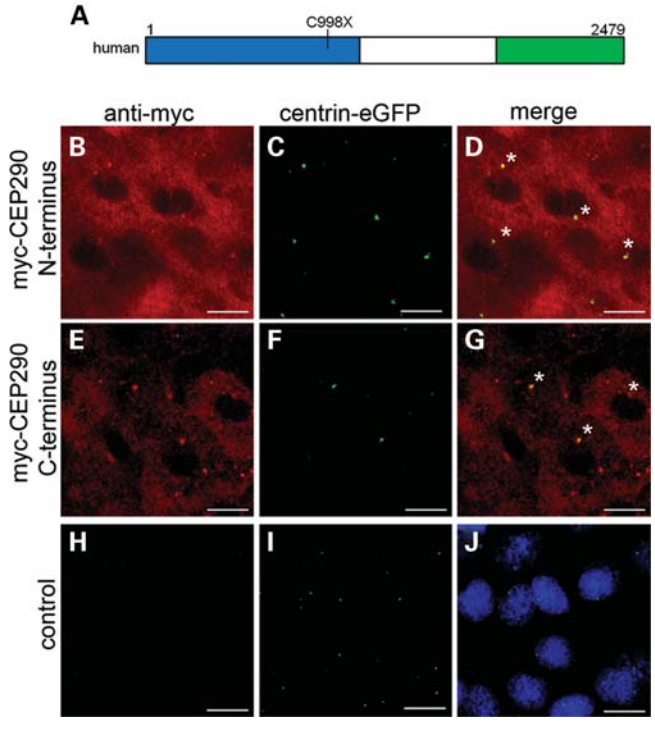

Figure 5. Cellular localization of the N-terminal and the C-terminal truncations of the human CEP290 protein. (**A**) Schematic of wild-type full-length human CEP290 protein with the N-terminal construct highlighted in blue (amino acids 1–1059) and the C-terminal construct highlighted in green (amino acids 1765–2479). The location of the common LCA human mutation, C998X, is noted. (**B**–**J**) Immunohistochemistry at 50% epiboly of N-terminal and C-terminal human myc-tagged CEP290 constructs and control centrin-eGFP only injected embryo. Scale bars = 10 μm. (B, E and H) Anti-myc immunoactivity (red). (C, F and I) Centrin-eGFP (green) labeling the centrioles. (D and G) Co-localization of centrin-eGFP and anti-myc straining revealing localization of both the N-terminal and the C-terminal regions of the CEP290 protein in the cytoplasm and paracentriolar. Asterisks mark co-localization of myc-CEP290 and centrin-eGFP. (J) Serves as a background control for anti-myc and florescent secondary immunoreactivity. Nuclei are labeled with ToPro3 (blue).

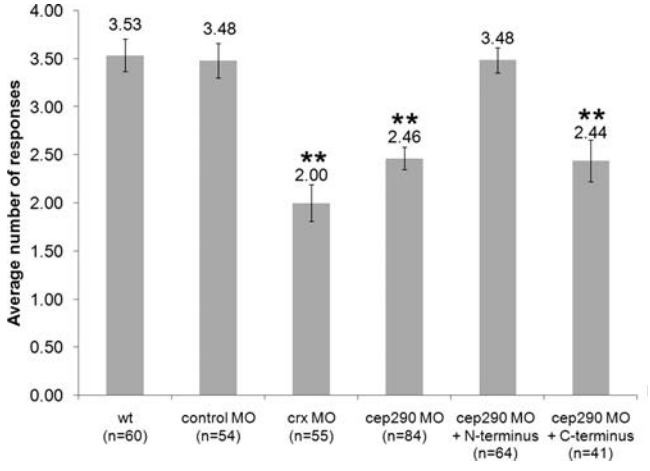

Figure 6. Rescue of the *cep290* morphant vision defect. Vision startle response assay for wild-type, control-injected, *cep290* morphants and rescue experiments. Experimental group and the number of embryos (*n*) are noted on the *x*-axis. The N-terminal RNA is sufficient to rescue the *cep290* morphant vision defect. $^{**}P < 0.01$, ANOVA with Tukey when compared with wild-type.

homozygous carriers (17). It is thought that these patients present with non-syndromic LCA because there is enough wild-type transcript present that other organ systems are unaffected (17). Consistent with this hypothesis, we observe that the penetrance of the curly body axis, as well as the severity of the KV defect and melanosome transport delay, is MO dose-dependent. We also show that although the splice-block MO does induce an intron inclusion, there is still some wild-type transcript present (Fig. 2C). Due to the lack of a CEP290 antibody that specifically recognizes the endogenous full-length or the N terminus of the protein in zebrafish, we cannot determine if the truncated protein is expressed from this aberrantly spliced transcript. However, since MO-injected embryos that do not show the curly body axis still have visual impairment, it is likely that levels of cep290 are sufficient for normal axis development but are not sufficient for normal visual function.

Our finding that the expression of only the N-terminal region of the CEP290 protein is sufficient to rescue the vision defect suggests that domains within this region are able to interact with their retina-specific binding partners to allow visual function. The ability of the N-terminal region of the human CEP290 to rescue the vision defect observed in *cep290* knockdown zebrafish embryos appears to be inconsistent with two existing animal models, the *rd16* mouse and the rdAc cat. Mutations in these model systems are found in the C-terminal region, suggesting that it is this region of the protein that is required for vision. Possible explanations for this inconsistency include that the mutant Cep290 protein in the mouse and cat models is unstable and degraded, folds in such a manner as to affect the structure of the N-terminal region resulting in alteration of binding properties or results in changes in protein localization. It has been shown in *rd16* mice that there is a reduced amount of the mutant Cep290 protein; moreover, the mutant Cep290 protein has a higher than normal affinity for RPGR, and the RPGR protein aberrantly localizes to the photoreceptor inner segment (4).

In human patients, there are several mutations found within the N-terminal region of CEP290 that result in LCA, including the mutation modeled in our study (2,3,16,17). This human mutation analysis suggests that regions outside that of the C terminus have a role in regulating binding to interacting proteins required for proper vision. The identification of NPHP protein complexes that interact with proteins known to affect vision has highlighted a molecular pathway to be further investigated for its role in the retina (19). Here, we have found that NPHP2 binds to only the N-terminal fragment of CEP290, which rescues the vision defect, but not the C-terminal construct, which suppresses the melanosome transport delay. This differential binding to restore individual phenotypes is an example of tissue specificity of protein function and highlights the importance of examining molecular pathways in a tissue-specific manner. Together, these ideas corroborate a hypothesis by Murga-Zamalloa *et al*. (19), in which the authors pose that the severity of a disease phenotype is the result of the degree to which individual complexes are disrupted.

Table 2. Compiled data set of KV, melanosome transport and vision startle response assay results for rescue experiments

Experimental group	KV (%)	MT (min) ± SE	Vision (responses) ± SE
Wild-type	5.2	1.51 ± 0.07	3.53 ± 0.17
control MO (10 ng)	8.3	1.52 ± 0.06	3.48 ± 0.18
cep290 MO (8 ng)	18.2^{++}	2.10 ± 0.10**	2.46 ± 0.12**
cep290 MO (8 ng) + N terminus (1.8 ng)	22.6^{++}	2.05 ± 0.10**	3.48 ± 0.13
cep290 MO (8 ng) + C terminus (0.6 ng)	15.4^{++}	1.82 ± 0.07	2.44 ± 0.22**

$^{++}$Fisher's Exact test $P < 0.01$.
**ANOVA with Tukey $P < 0.01$.

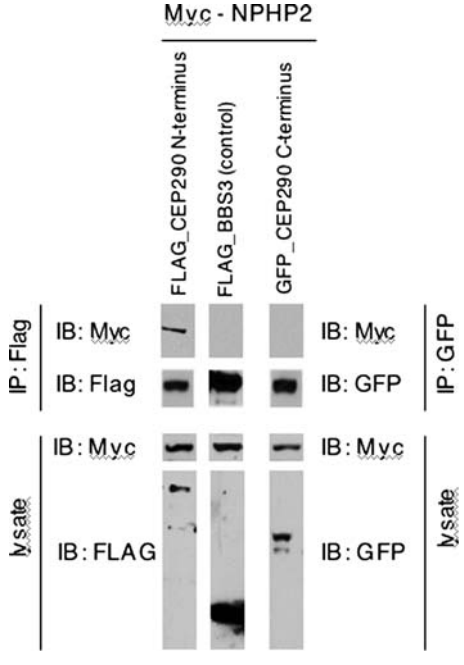

Figure 7. The N-terminal region of CEP290 interacts with NPHP2. FLAG or GFP-tagged CEP290 expression constructs and Myc-tagged NPHP2 were transfected into HEK293T cells, and lysates were subjected to co-IP and immunoblotting (IB). Expression of each component in the lysate is found in the bottom two panels. IPs were analyzed by SDS–PAGE and immunoblotting using the Myc antibody and either the FLAG or the GFP antibodies shown in the upper two panels. Myc-NPHP2 was only co-immunoprecipitated from cells expressing N-terminal CEP290 fragment (top panel). FLAG-tagged BBS3 served as a negative control.

In summary, we have identified a region of the CEP290 protein that is sufficient to restore visual function in *cep290* knockdown zebrafish embryos. This construct rescues the vision defect, suggesting domain and tissue-type specificity for this region of the protein. Although gene therapy vectors are being generated that are able to package large genes such as the entire *CEP290* coding region (38), the functional characterization of a smaller portion of this protein sufficient to restore vision provides valuable information that can be used for potential treatments of LCA patients. Finally, we have begun to examine interacting partners with CEP290 to determine how this shortened construct is able to functionally rescue vision. We have shown that NPHP2, a known component of an identified protein complex in the retina, can bind the N-terminal construct that rescues the vision defect but not the C-terminal piece. Future work will be focused on elucidating the mechanism by which the N-terminal region of CEP290 functions within the retina.

MATERIALS AND METHODS

Animal care

Zebrafish embryos were collected from natural spawning and maintained under standard conditions (39). Embryos were developmentally staged as described previously (40).

Reverse transcriptase–polymerase chain reaction

RNA was extracted from pools of wild-type embryos at the following stages: 1–128 cells (maternal stage), 8–10 somites, 48 hpf and 5 dpf, as well as the adult retina and whole eye. cDNA was synthesized using oligo-dT primers. Gene expression was evaluated using the following primers whose location in the *cep290* gene is depicted in Figure 2A. *β-actin* expression served as a control.

cep290—primer F1: 5′-GGAACAGGCCTTTGAAAACA-3′
cep290—primer R1: 5′-GCAAACTTGGTCTCCAGCTC-3′
β-actin—primer F: 5′-TCAGCCATGGATGATGAAAT-3′
β-actin —primer R: 5′-GGTCAGGATCTTCATGAGGT-3′

Whole-mount *in situ* hybridization

A large 5′ segment of the zebrafish *cep290* open reading frame (Ensemble v8: ENSDART00000090921) was TA cloned into PCRII vector (Invitrogen) from a multistage pool of embryonic cDNA. After digesting the vector with *Dra*I, a digoxigenin-UTP-labeled RNA probe was synthesized using SP6 polymerase (Roche). The resulting ∼1.9 kb antisense probe corresponds to 2784–4656 bp of the zebrafish *cep290* gene. Whole-mount *in situ* hybridization was performed as described previously (41). Control embryos had no antisense probe added in the reaction. For section analysis of the retina, embryos were embedded in optimal cutting temperature compound and 15 μm cryosections were collected.

cep290—primer F2: 5′GACTGGCAATCTCAGCATCAGT-3′
cep290—primer R2: 5′-GCGAGCCTTTCCTAGAAGGT-3′

MO knockdown

The antisense splice site MO was designed and purchased from Gene Tools. The MO was air pressure injected into 1–4-cell embryos at concentrations ranging from 5 to 10 ng. The efficiency of transcript knockdown was assessed by RT–PCR (described above) using cDNA generated from pools of *cep290* morphants with only the straight body axis phenotype at the following stages: 8–10 somites, 72 hpf and 5 dpf.

Standard control MO: 5′-CCTCTTACCTCAGTTACAATT TATA-3′
cep290 MO: 5′-TTGATGTGTACCAGTTGTGCTGATG-3′

Analysis of KV size and melanosome transport time

The KV size was assessed on live embryos between the 6–12-somite stages of development as described previously (23). Embryos with a KV smaller than the width of the notochord were recorded as abnormal. The melanosome transport assay was performed as described previously (23). Briefly, 5 dpf dark-adapted embryos were treated with epinephrine (500 μg/ml, Sigma E4375), and the quantity of time that it took the melanosomes to traffic from the periphery of the cell to their perinuclear location was recorded. Embryos were imaged live using a stereoscope with a Zeiss Axiocam camera.

Histological analysis

To minimize the pigmentation of the retinal pigmented epithelium in order to view the outer segments of the photoreceptor cells, embryos were maintained in 0.003% phenylthiourea beginning at 80% epiboly and then fixed in 4% paraformaldehyde in phosphate-buffered saline (PBS). Gross morphology of the retinas was evaluated with standard H&E staining.

Vision startle response assay

The vision-evoked startle-response behavioral assay was performed as described previously (26,34,35). In brief, 5 dpf zebrafish embryos were light adapted, and the visual stimulus of a 1 s block in bright light intensity was performed under a dissecting microscope. A positive visual response was recorded if the embryo made an abrupt change in swimming behavior within 1 s of the light intensity change. Five trials were performed spaced 30 s apart followed by the mechanical stimulus of probing embryos with the tip of a blunt needle. Embryos that did not respond to the mechanical stimulus were not included in the analysis.

DNA constructs

The fragments encoding the N-terminal (1–1059 amino acids) and the C-terminal regions (1765–2479 amino acids) of human wild-type *CEP290* (NCBI Reference Sequence: NG_008417.1) were amplified from human retina cDNA (Clonetech), TA cloned into the Gateway vector system (Invitrogen) and sequence confirmed. Subsequently, the genes were recombined into gateway expression vectors with an N-terminal 6× myc tag.

CEP290—primer N-terminal F: 5′-ATGCCACCTAATA TAAACTGG-3′
CEP290—primer N-terminal R: 5′-TCATATTTTTTTT GAAATGGAAACAATGTC-3′
CEP290—primer C-terminal F: 5′-ATGTCTGCAACTTCT CAAAAAGAG-3′
CEP290—primer C-terminal R: 5′-TTAGTAAATGGG GAAATTAACAGG-3′

Protein localization and rescue experiments

N-terminally tagged human myc-*CEP290* RNA was synthesized using the mMessage mMachine transcription kit (Ambion) and injected into 1–2-cell embryos. Whole-mount immunohistochemistry was performed on 50% epiboly stage embryos as described (42) using an anti-myc antibody (9E10, Santa Cruz) and fluorescent secondaries (Alexa Fluor 568, Molecular Probes). The centrin-eGFP was detected by direct GFP fluorescence. For rescue experiments, the synthetic RNA was co-injected with the *cep*290 MO.

Cell culture and immunofluorescence microscopy

ARPE-19 cells were maintained in DMEM/F12 media (Invitrogen) supplemented with 10% fetal bovine serum (FBS) and seeded on glass coverslips in 24-well plates. To induce ciliogenesis, cells were shifted to serum-free medium 24 h after seeding and further incubated for 48 h. Cells were fixed with methanol for 10 min at 4°C, blocked with 5% bovine serum albumin and 3% normal goat serum and stained with indicated primary antibodies. Alexa Fluor 488 goat anti-rabbit immunoglobulin (Ig) G (Invitrogen) and 568 goat anti-mouse IgG (Invitrogen) were used to detect the primary antibodies. Coverslips were mounted on Vecta-Shield mounting with DAPI (Vector Lab), and images were taken with an Olympus 1X71 inverted microscope. Antibodies were purchased from the following sources: mouse monoclonal antibodies against γ-tubulin (GTU-88, Sigma) and acetylated-tubulin (T7451, Sigma); rabbit polyclonal antibody against Myc (ab9106, Abcam).

Cell culture and IP

HEK293T cells were grown in Dulbecco's modification of Eagle's medium (DMEM) (Invitrogen) supplemented with 10% FBS (Invitrogen). For individual protein–protein interaction studies, cells were transfected in 6-well plates with total 1.5 μg indicated plasmids using Lipofectamine Reagent (Invitrogen). After 30 h of incubation, cells were lysed in the lysis buffer (PBS, 0.5% Triton X-100) supplemented with Complete Protease Inhibitor Mixture (Roche Applied Science). Lysates were immunoprecipitated with anti-Flag and anti-GFP antibodies conjugated to agarose beads for 4 h at 4°C. Beads were washed in the lysis buffer four times, and precipitated proteins were analyzed by sodium dodecyl sulfate-polyacrylamide gel electrophoresis (SDS–PAGE) and western blotting following a standard protocol. Experiments were repeated 2–3 times, with similar results. Antibodies were purchased from the following sources: mouse monoclonal antibodies against Myc (9E10; Santa Cruz), FLAG (M2; Sigma) and GFP (18A11, Santa Cruz).

SUPPLEMENTARY MATERIAL

Supplementary Material is available at *HMG* online.

ACKNOWLEDGEMENTS

We thank Dr Caren Norden (University of Cambridge) for the gift of the zebrafish *centrin* fused to *eGFP* and Dr Darryl Nishmura and Dr Qihong Zhang (University of Iowa) for their technical expertise.

Conflict of Interest statement. None declared.

FUNDING

This work was supported by the National Institute of Health [R01CA112369 to D.C.S., R01EY110298 and R01EY017168 to V.C.S. and E.M.S.]; the Grousbeck Family Foundation; the Roy J. Carver Charitable Trust; the Foundation Fighting Blindness; Research to Prevent Blindness; and an Iowa Cardiovascular Center Institutional Research Fellowship [T32HL0712135 to L.M.B.]. V.C.S. and E.M.S. are Investigators of the Howard Hughes Medical Institute. Funding to pay the Open Access publication charges for this article was provided by the Howard Hughes Medical Institute.

REFERENCES

1. Sayer, J.A., Otto, E.A., O'Toole, J.F., Nurnberg, G., Kennedy, M.A., Becker, C., Hennies, H.C., Helou, J., Attanasio, M., Fausett, B.V. *et al.* (2006) The centrosomal protein nephrocystin-6 is mutated in Joubert syndrome and activates transcription factor ATF4. *Nat. Genet.*, **38**, 674–681.
2. Coppieters, F., Lefever, S., Leroy, B.P. and De Baere, E. (2010) CEP290, a gene with many faces: mutation overview and presentation of CEP290base. *Hum. Mutat.*, **31**, 1097–1108.
3. Frank, V., den Hollander, A.I., Bruchle, N.O., Zonneveld, M.N., Nurnberg, G., Becker, C., Du Bois, G., Kendziorra, H., Roosing, S., Senderek, J. *et al.* (2008) Mutations of the CEP290 gene encoding a centrosomal protein cause Meckel-Gruber syndrome. *Hum. Mutat.*, **29**, 45–52.
4. Chang, B., Khanna, H., Hawes, N., Jimeno, D., He, S., Lillo, C., Parapuram, S.K., Cheng, H., Scott, A., Hurd, R.E. *et al.* (2006) In-frame deletion in a novel centrosomal/ciliary protein CEP290/NPHP6 perturbs its interaction with RPGR and results in early-onset retinal degeneration in the rd16 mouse. *Hum. Mol. Genet.*, **15**, 1847–1857.
5. Besharse, J.C., Baker, S.A., Luby-Phelps, K. and Pazour, G.J. (2003) Photoreceptor intersegmental transport and retinal degeneration: a conserved pathway common to motile and sensory cilia. *Adv. Exp. Med. Biol.*, **533**, 157–164.
6. Krock, B.L. and Perkins, B.D. (2008) The intraflagellar transport protein IFT57 is required for cilia maintenance and regulates IFT-particle-kinesin-II dissociation in vertebrate photoreceptors. *J. Cell. Sci.*, **121**, 1907–1915.
7. Luby-Phelps, K., Fogerty, J., Baker, S.A., Pazour, G.J. and Besharse, J.C. (2008) Spatial distribution of intraflagellar transport proteins in vertebrate photoreceptors. *Vision Res.*, **48**, 413–423.
8. Pazour, G.J., Baker, S.A., Deane, J.A., Cole, D.G., Dickert, B.L., Rosenbaum, J.L., Witman, G.B. and Besharse, J.C. (2002) The intraflagellar transport protein, IFT88, is essential for vertebrate photoreceptor assembly and maintenance. *J. Cell Biol.*, **157**, 103–113.
9. Tsujikawa, M. and Malicki, J. (2004) Intraflagellar transport genes are essential for differentiation and survival of vertebrate sensory neurons. *Neuron*, **42**, 703–716.
10. Young, R.W. (1968) Passage of newly formed protein through the connecting cilium of retina rods in the frog. *J. Ultrastruct. Res.*, **23**, 462–473.
11. Deretic, D., Williams, A.H., Ransom, N., Morel, V., Hargrave, P.A. and Arendt, A. (2005) Rhodopsin C terminus, the site of mutations causing retinal disease, regulates trafficking by binding to ADP-ribosylation factor 4 (ARF4). *Proc. Natl Acad. Sci. USA*, **102**, 3301–3306.
12. Pazour, G.J. and Rosenbaum, J.L. (2002) Intraflagellar transport and cilia-dependent diseases. *Trends Cell Biol.*, **12**, 551–555.
13. den Hollander, A.I., Roepman, R., Koenekoop, R.K. and Cremers, F.P. (2008) Leber congenital amaurosis: genes, proteins and disease mechanisms. *Prog. Retin. Eye Res.*, **27**, 391–419.
14. Pasadhika, S., Fishman, G.A., Stone, E.M., Lindeman, M., Zelkha, R., Lopez, I., Koenekoop, R.K. and Shahidi, M. (2010) Differential macular morphology in patients with RPE65-, CEP290-, GUCY2D-, and AIPL1-related Leber congenital amaurosis. *Invest. Ophthalmol. Vis. Sci.*, **51**, 2608–2614.
15. Stone, E.M. (2007) Leber congenital amaurosis—a model for efficient genetic testing of heterogeneous disorders: LXIV Edward Jackson Memorial Lecture. *Am. J. Ophthalmol.*, **144**, 791–811.
16. Perrault, I., Delphin, N., Hanein, S., Gerber, S., Dufier, J.L., Roche, O., Defoort-Dhellemmes, S., Dollfus, H., Fazzi, E., Munnich, A. *et al.* (2007) Spectrum of NPHP6/CEP290 mutations in Leber congenital amaurosis and delineation of the associated phenotype. *Hum. Mutat.*, **28**, 416.
17. den Hollander, A.I., Koenekoop, R.K., Yzer, S., Lopez, I., Arends, M.L., Voesenek, K.E., Zonneveld, M.N., Strom, T.M., Meitinger, T., Brunner, H.G. *et al.* (2006) Mutations in the CEP290 (NPHP6) gene are a frequent cause of Leber congenital amaurosis. *Am. J. Hum. Genet.*, **79**, 556–561.
18. Menotti-Raymond, M., David, V.A., Schaffer, A.A., Stephens, R., Wells, D., Kumar-Singh, R., O'Brien, S.J. and Narfstrom, K. (2007) Mutation in CEP290 discovered for cat model of human retinal degeneration. *J. Hered.*, **98**, 211–220.
19. Murga-Zamalloa, C.A., Desai, N.J., Hildebrandt, F. and Khanna, H. (2010) Interaction of ciliary disease protein retinitis pigmentosa GTPase regulator with nephronophthisis-associated proteins in mammalian retinas. *Mol. Vis.*, **16**, 1373–1381.
20. Leitch, C.C., Zaghloul, N.A., Davis, E.E., Stoetzel, C., Diaz-Font, A., Rix, S., Alfadhel, M., Lewis, R.A., Eyaid, W., Banin, E. *et al.* (2008) Hypomorphic mutations in syndromic encephalocele genes are associated with Bardet-Biedl syndrome. *Nat. Genet.*, **40**, 443–448.
21. Schafer, T., Putz, M., Lienkamp, S., Ganner, A., Bergbreiter, A., Ramachandran, H., Gieloff, V., Gerner, M., Mattonet, C., Czarnecki, P.G. *et al.* (2008) Genetic and physical interaction between the NPHP5 and NPHP6 gene products. *Hum. Mol. Genet.*, **17**, 3655–3662.
22. Tobin, J.L. and Beales, P.L. (2008) Restoration of renal function in zebrafish models of ciliopathies. *Pediatr. Nephrol.*, **23**, 2095–2099.
23. Yen, H.J., Tayeh, M.K., Mullins, R.F., Stone, E.M., Sheffield, V.C. and Slusarski, D.C. (2006) Bardet-Biedl syndrome genes are important in retrograde intracellular trafficking and Kupffer's vesicle cilia function. *Hum. Mol. Genet.*, **15**, 667–677.
24. Chiang, A.P., Beck, J.S., Yen, H.J., Tayeh, M.K., Scheetz, T.E., Swiderski, R.E., Nishimura, D.Y., Braun, T.A., Kim, K.Y., Huang, J. *et al.* (2006) Homozygosity mapping with SNP arrays identifies TRIM32, an E3 ubiquitin ligase, as a Bardet-Biedl syndrome gene (BBS11). *Proc. Natl Acad. Sci. USA*, **103**, 6287–6292.
25. Tayeh, M.K., Yen, H.J., Beck, J.S., Searby, C.C., Westfall, T.A., Griesbach, H., Sheffield, V.C. and Slusarski, D.C. (2008) Genetic interaction between Bardet-Biedl syndrome genes and implications for limb patterning. *Hum. Mol. Genet.*, **17**, 1956–1967.
26. Pretorius, P.R., Baye, L.M., Nishimura, D.Y., Searby, C.C., Bugge, K., Yang, B., Mullins, R.F., Stone, E.M., Sheffield, V.C. and Slusarski, D.C. (2010) Identification and functional analysis of the vision-specific BBS3 (ARL6) long isoform. *PLoS Genet.*, **6**, e1000884.
27. Essner, J.J., Amack, J.D., Nyholm, M.K., Harris, E.B. and Yost, H.J. (2005) Kupffer's vesicle is a ciliated organ of asymmetry in the zebrafish embryo that initiates left-right development of the brain, heart and gut. *Development*, **132**, 1247–1260.
28. Kishimoto, N., Cao, Y., Park, A. and Sun, Z. (2008) Cystic kidney gene seahorse regulates cilia-mediated processes and Wnt pathways. *Dev. Cell*, **14**, 954–961.
29. Aspengren, S., Skold, H.N. and Wallin, M. (2009) Different strategies for color change. *Cell Mol. Life Sci.*, **66**, 187–191.
30. Marks, M.S. and Seabra, M.C. (2001) The melanosome: membrane dynamics in black and white. *Nat. Rev. Mol. Cell Biol.*, **2**, 738–748.
31. Skold, H.N., Norstrom, E. and Wallin, M. (2002) Regulatory control of both microtubule- and actin-dependent fish melanosome movement. *Pigment. Cell Res.*, **15**, 357–366.
32. Nascimento, A.A., Roland, J.T. and Gelfand, V.I. (2003) Pigment cells: a model for the study of organelle transport. *Annu. Rev. Cell Dev. Biol.*, **19**, 469–491.
33. Cideciyan, A.V., Aleman, T.S., Jacobson, S.G., Khanna, H., Sumaroka, A., Aguirre, G.K., Schwartz, S.B., Windsor, E.A., He, S., Chang, B. *et al.* (2007) Centrosomal-ciliary gene CEP290/NPHP6 mutations result in blindness with unexpected sparing of photoreceptors and visual brain: implications for therapy of Leber congenital amaurosis. *Hum. Mutat.*, **28**, 1074–1083.
34. Easter, S.S. Jr. and Nicola, G.N. (1996) The development of vision in the zebrafish (*Danio rerio*). *Dev. Biol.*, **180**, 646–663.

35. Nishimura, D.Y., Baye, L.M., Perveen, R., Searby, C.C., Avila-Fernandez, A., Pereiro, I., Ayuso, C., Valverde, D., Bishop, P.N., Manson, F.D. *et al.* (2010) Discovery and functional analysis of a retinitis pigmentosa gene, C2ORF71. *Am. J. Hum. Genet.*, **86**, 686–695.
36. Otto, E.A., Loeys, B., Khanna, H., Hellemans, J., Sudbrak, R., Fan, S., Muerb, U., O'Toole, J.F., Helou, J., Attanasio, M. *et al.* (2005) Nephrocystin-5, a ciliary IQ domain protein, is mutated in Senior-Loken syndrome and interacts with RPGR and calmodulin. *Nat. Genet.*, **37**, 282–288.
37. O'Toole, J.F., Otto, E.A., Frishberg, Y. and Hildebrandt, F. (2006) Retinitis pigmentosa and renal failure in a patient with mutations in INVS. *Nephrol. Dial. Transplant*, **21**, 1989–1991.
38. Allocca, M., Doria, M., Petrillo, M., Colella, P., Garcia-Hoyos, M., Gibbs, D., Kim, S.R., Maguire, A., Rex, T.S., Di Vicino, U. *et al.* (2008) Serotype-dependent packaging of large genes in adeno-associated viral vectors results in effective gene delivery in mice. *J. Clin. Invest.*, **118**, 1955–1964.
39. Westerfield, M. (1995) *The Zebrafish Book*. University of Oregon Press, Eugene, OR.
40. Kimmel, C.B., Ballard, W.W., Kimmel, S.R., Ullmann, B. and Schilling, T.F. (1995) Stages of embryonic development of the zebrafish. *Dev. Dyn.*, **203**, 253–310.
41. Thisse, C., Thisse, B., Schilling, T.F. and Postlethwait, J.H. (1993) Structure of the zebrafish snail1 gene and its expression in wild-type, spadetail and no tail mutant embryos. *Development*, **119**, 1203–1215.
42. Westfall, T.A., Brimeyer, R., Twedt, J., Gladon, J., Olberding, A., Furutani-Seiki, M. and Slusarski, D.C. (2003) Wnt-5/pipetail functions in vertebrate axis formation as a negative regulator of Wnt/beta-catenin activity. *J. Cell Biol.*, **162**, 889–898.